# Nightside ionosphere of Mars: Radar soundings by the Mars Express spacecraft

F. Němec,[1] D. D. Morgan,[1] D. A. Gurnett,[1] and F. Duru[1]

Received 26 May 2010; revised 23 September 2010; accepted 6 October 2010; published 14 December 2010.

[1] We present results of a survey of the nightside ionosphere of Mars as observed by Mars Advanced Radar for Subsurface and Ionospheric Sounding (MARSIS) on board the Mars Express spacecraft. The occurrence rate of the nightside ionosphere is studied as a function of solar zenith angle (SZA), magnetic field magnitude, and magnetic field inclination. It is shown that at locations with weak crustal magnetic fields the occurrence rate of the nightside ionosphere decreases with increasing SZA up to about 125°, suggesting that plasma transport from the dayside plays a crucial role in its formation. However, at locations with strong crustal magnetic fields, the dependence on SZA is no longer apparent and the inclination of magnetic field becomes a crucial parameter: the occurrence rate of the nightside ionosphere is more than 4 times larger at locations with nearly vertical magnetic fields as compared to the locations with nearly horizontal magnetic fields. This indicates that impact ionization by precipitating electrons is the main ionization source at these locations. Observed peak electron densities are less than $2 \times 10^4$ cm$^{-3}$ in the vast majority of cases. Lower estimates of altitudes of peak electron densities are mostly between 100 and 150 km.

**Citation:** Němec, F., D. D. Morgan, D. A. Gurnett, and F. Duru (2010), Nightside ionosphere of Mars: Radar soundings by the Mars Express spacecraft, *J. Geophys. Res.*, *115*, E12009, doi:10.1029/2010JE003663.

## 1. Introduction

[2] It has been shown that the dayside ionosphere of Mars can be (at least to a first approximation and near the ionospheric peak) relatively well described by classical Chapman theory [*Chapman*, 1931]; that is, it is formed primarily due to the photoionization of atmospheric neutrals by incoming solar radiation [*Gurnett et al.*, 2005, 2008; *Morgan et al.*, 2008]. However, our understanding of the formation of the nightside ionosphere of Mars is more limited.

[3] *Zhang et al.* [1990] used the Viking spacecraft and the radio occultation method to find that for about 60% of available profiles at solar zenith angles (SZA) between 90° and 125° no significant peak can be identified, suggesting that the electron density in the nightside ionosphere is often too low to be detected. For those cases in which it was detected, the average peak electron density was about $5 \times 10^3$ cm$^{-3}$. This is below the peak electron densities in the subsolar region by a factor of more than 30 [*Morgan et al.*, 2008]. The altitudes of peak electron densities detected by *Zhang et al.* [1990] fell mostly in the range of 150–180 km, as compared to the peak altitude near the subsolar point of about 130 km [*Morgan et al.*, 2008]. *Safaeinili et al.* [2007] measured the total electron content (TEC) of the Martian ionosphere using MARSIS surface echoes. Their results indicated that for SZAs within 100°–130° there is an enhancement in the TEC over regions where the magnetic field is vertical. *Gurnett et al.* [2008] reported that the peak electron densities observed by the MARSIS instrument at SZAs between about 90°–110° are highly irregular and larger than the ones corresponding to a Chapman profile. Moreover, they found that the ionospheric echoes in this region are often very diffuse (i.e., fuzzy and poorly defined) and occur in highly localized regions. Overall, there is a dearth of nightside ionospheric observations and the deep nightside ionosphere (SZA > 125°) remains completely unexplored [*Withers*, 2009].

[4] Concerning recent modeling efforts, *Fox et al.* [1993] derived upper limits of peak electron densities of the Martian nightside ionosphere, assuming its formation both by electron precipitation and plasma transport from the dayside. The computed electron density peaks were in the range 1.3–$1.9 \times 10^4$ cm$^{-3}$ at altitudes of 159 to 179 km. *Fillingim et al.* [2007] used an electron transport model and Mars Global Surveyor observations of electron spectra to investigate the effect of electron precipitation on the electron density in the nightside ionosphere of Mars. They calculated vertical profiles of the ionization rates and electron densities, and showed that the maximum number density depends significantly on the electron spectrum used. The reported difference was by a factor of 3 larger for an accelerated electron spectrum as compared to a typical tail spectrum. Subsequently, *Lillis et al.* [2009] used a Monte Carlo method to

[1]Department of Physics and Astronomy, University of Iowa, Iowa City, Iowa, USA.


0148-0227/10/2010JE003663

investigate the coupled effects of crustal magnetic field gradients and precipitating electron pitch angle distributions. Including such effects, particularly in the case of non-isotropic pitch angle distributions, was found to be essential in accurately predicting ionization rates and electron density profiles.

[5] In the present study we report results of a survey of the nightside ionosphere of Mars based on more than 4 years of measurements performed by the Mars Advanced Radar for Subsurface and Ionospheric Sounding (MARSIS) on board the Mars Express spacecraft. The occurrence rate of the nightside ionosphere, peak electron densities and altitudes of the detected peaks are determined, and the influence of SZA, magnetic field magnitude and inclination of magnetic field are studied.

[6] The data set used in the study and a brief description of the MARSIS instrument are described in section 2. The results obtained are presented in section 3 and discussed in section 4. Finally, section 5 contains a short summary of the main results.

## 2. Data Set

[7] MARSIS is an instrument designed for topside ionospheric sounding. The Mars Express spacecraft is in an eccentric orbit around Mars with a periapsis altitude of about 275 km, an apoapsis altitude of about 11000 km, an orbital inclination 86°, and an orbital period of 6.75 h [*Chicarro et al.*, 2004]. The MARSIS radar sounder uses a 40 m tip-to-tip electric dipole antenna for transmitting the sounding wave and for reception of its reflection.

[8] The basic idea of ionospheric sounding is that ordinary mode electromagnetic waves cannot propagate at frequencies lower than the plasma frequency $f_p$, which is given approximately by

$$f_p = 8980\sqrt{n_e} \quad (1)$$

where $f_p$ is in Hz and $n_e$ is the electron density in cm$^{-3}$. In the case of extraordinary mode waves, the magnetic field has an additional effect. Taking into account that the electron gyrofrequency is generally much lower than the electron plasma frequency, it is possible to show that the reflection occurs at a frequency that is higher by half the electron gyrofrequency [*Piggott and Rawer*, 1972]. However, in the case of Mars, the magnetic field is so small that the difference between the reflection frequencies is negligible, so there is no need to distinguish between the two modes. For normal incidence a short pulse transmitted at a fixed frequency $f$ reflects at boundaries where $f_p = f$. By measuring the time delay $\Delta t$ between the transmission of the pulse and the time when the echo is received, it is possible to calculate the range to the reflection point. By varying the frequency, the range to the reflection point can be determined as a function of frequency. Finally, it is clear that signals at frequencies larger than the plasma frequency of the peak electron density in the ionosphere never meet a boundary $f_p = f$ and do not undergo an ionospheric reflection. When not absorbed by the ionosphere, such pulses generate surface reflections.

[9] During operation in the ionospheric sounding mode the MARSIS transmitter steps through 160 quasi-logarithmically spaced frequencies ($\Delta F/F \approx 2\%$) from 0.1 to 5.5 MHz. At each step a 91 $\mu$s long quasi-sinusoidal pulse is transmitted and the intensities of any detected echoes are recorded in 80 equally spaced time delay bins over an interval of 7.31 ms. The time duration of a scan over all 160 sounding frequencies is 1.26 s. Such a scan is repeated every 7.54 s. Taking into account equation (1) and the range of sounding frequencies used, peak electron densities spanning from about 124 cm$^{-3}$ to 3.75 × 10$^5$ cm$^{-3}$ theoretically can be detected. However, since the radiated power of the dipole antenna falls off rapidly at frequencies below about 500 kHz, it is usually not possible to detect peak electron densities lower than about 5000 cm$^{-3}$. Ionospheres with lower electron densities are unlikely to be detected by MARSIS. More detailed descriptions of the MARSIS instrument are given by *Picardi et al.* [2004] and *Jordan et al.* [2009].

[10] A plot of the color-coded intensity of detected echoes as a function of the time delay $\Delta t$ and frequency $f$ is called an ionogram and represents the principal output of the MARSIS instrument. An example of an ionogram corresponding to an observation of the nightside ionosphere is shown in Figure 1. Two distinct features can be seen. The first of them, spanning frequencies from about 1 MHz to the upper frequency limit of the instrument, corresponds to the reflection from the surface of Mars [*Gurnett et al.*, 2005, 2008] and is not relevant to the topic of this paper. The shorter feature at smaller time delays observed in the frequency range about 0.6–1.0 MHz is the echo due to the reflection of the transmitted pulse from the nightside ionosphere and is the primary source of data for this study. As can be seen, it is nearly horizontal, with a quite sharp upper edge, but with a rather fuzzy bottom edge. The fuzzy bottom edge is a general feature of the nightside ionosphere echoes and will be discussed more in detail in section 4.

[11] We would like to point out that due to the specific shape of the echoes it is possible to characterize each of them by only three parameters: the minimum sounding frequency for which the echo was observed, the maximum sounding frequency for which the echo was observed and the time delay of the echo. Concerning the time delay of the echo, we are most interested in the minimum time delay of the echo (i.e., the upper sharp edge), which corresponds to the normal incidence of the transmitted signal, rather than in the maximum time delay of the echo (i.e., the fuzzy bottom edge): a more detailed discussion of this issue will be given in section 4.

[12] Since an automated detection algorithm was regarded to be infeasible, we have visually inspected all of the MARSIS ionograms from the beginning of the mission until the end of 2009 for the presence of nightside ionospheric echoes. We have focused only on the data measured at SZA > 107°, in order to assure that the ionosphere at a typical peak altitude of 150 km is in the shadow of the planet. Moreover, taking into account that the grazing incidence solar radiation at altitudes up to about 80 km above the Martian surface is absorbed, the ionosphere at these SZAs is not sunlit up to about 240 km. In addition, we have selected only those time intervals when the altitude of the Mars Express spacecraft is lower than 1100 km. Since the time delays of returning echoes are measured up to 7.31 ms this ensures that an ionospheric echo (if present) would be within the sampled time delay. Altogether, there were 1682 orbits with 30,523 ionograms that satisfy the above two conditions.

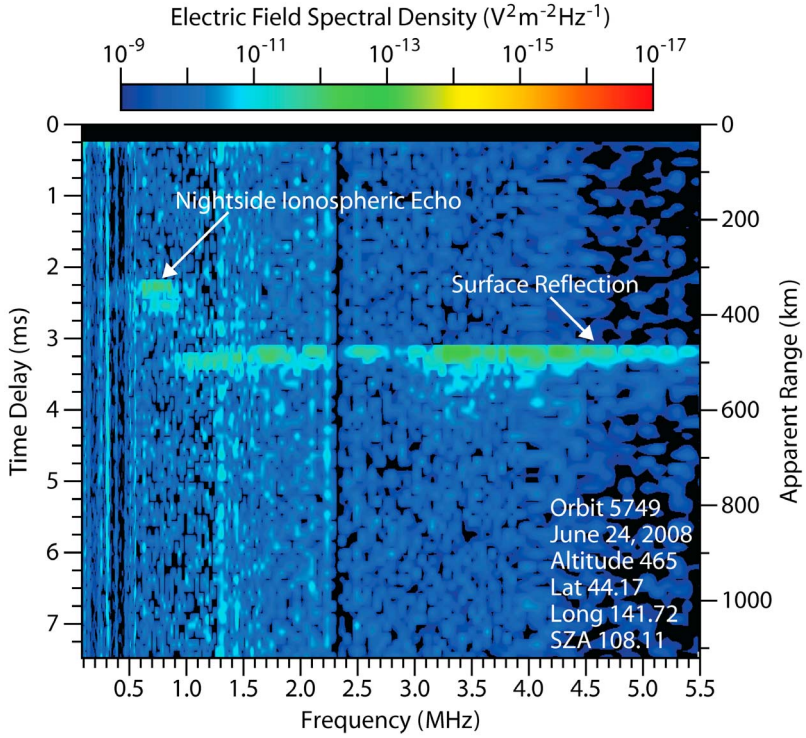


**Figure 1.** Example of an ionogram with a signature of the nightside ionosphere. Received intensity is color coded as a function of sounding frequency (abscissa) and time delay (left-hand ordinate) or apparent range (right-hand ordinate). The nightside ionospheric trace and surface reflection are labeled.

Among these, nightside ionospheric echoes were identified in 2857 ionograms (average occurrence rate of about 9 percent). For each echo, we have recorded the time of measurement, the minimum frequency of the observed ionospheric echo, the maximum frequency of the ionospheric echo and the time delay of the echo. We have also recorded the SZA, altitude, latitude, longitude, and local time for each observation.

## 3. Results

### 3.1. Occurrence Rate of the Nightside Ionosphere

[13] Figure 2a shows the geographic locations of all MARSIS measurements sampled in this study, while Figure 2b shows those geographic locations at which the nightside ionosphere was observed. It can be seen that both the measurements and the observed nightside ionospheres have good coverage in the area within ±50° from the equator, with more measurements being made in the southern hemisphere. The occurrence rate map of the nightside ionosphere calculated using 20° × 20° bins and the data from Figures 2a and 2b is shown in Figure 2c. Only the bins containing at least 100 measurements are plotted in order to eliminate the bins with poor data coverage. No obvious features are observed in the occurrence rate of the nightside ionosphere. Although the crustal magnetic fields in the northern and southern hemispheres are quite different (they are generally weaker in the northern hemisphere), nightside ionospheres were observed in both hemispheres.

[14] The occurrence rate of the nightside ionosphere as a function of SZA is shown in Figure 3. The red histogram represents the number of ionograms that contained a signature of the nightside ionosphere, while the dashed black histogram represents the total number of observations performed at a given SZA. Both histograms use a logarithmic scale spanning from 1 to 10,000 events. The scale on the right applies to the blue histogram, which represents the resulting occurrence rate of the nightside ionosphere, calculated as a ratio of the number of ionograms containing a signature of the ionospheric echo to the total number of the analyzed ionograms.

[15] The three panels were obtained for different magnitudes of the magnetic field. Since Mars Express does not have a magnetometer (although it is sometimes possible to perform measurements of magnetic field magnitude with MARSIS, see *Gurnett et al.* [2005]) and, moreover, since magnetic field data are needed at the same altitude in order to enable comparison between individual observations, we used the magnetic field model developed by *Cain et al.* [2003]. The magnetic field magnitudes were determined at an altitude of 400 km. This altitude was selected because that is where the great majority of data comprising the model were collected and where the model is most accurate, representing a reliable proxy for the magnetic field strength at ionospheric altitudes. In Figure 3a we present the solar zenith angle dependence of the detection and occurrence rates without regard to magnetic field. Figure 3b was obtained for regions with weak crustal magnetic fields (lower

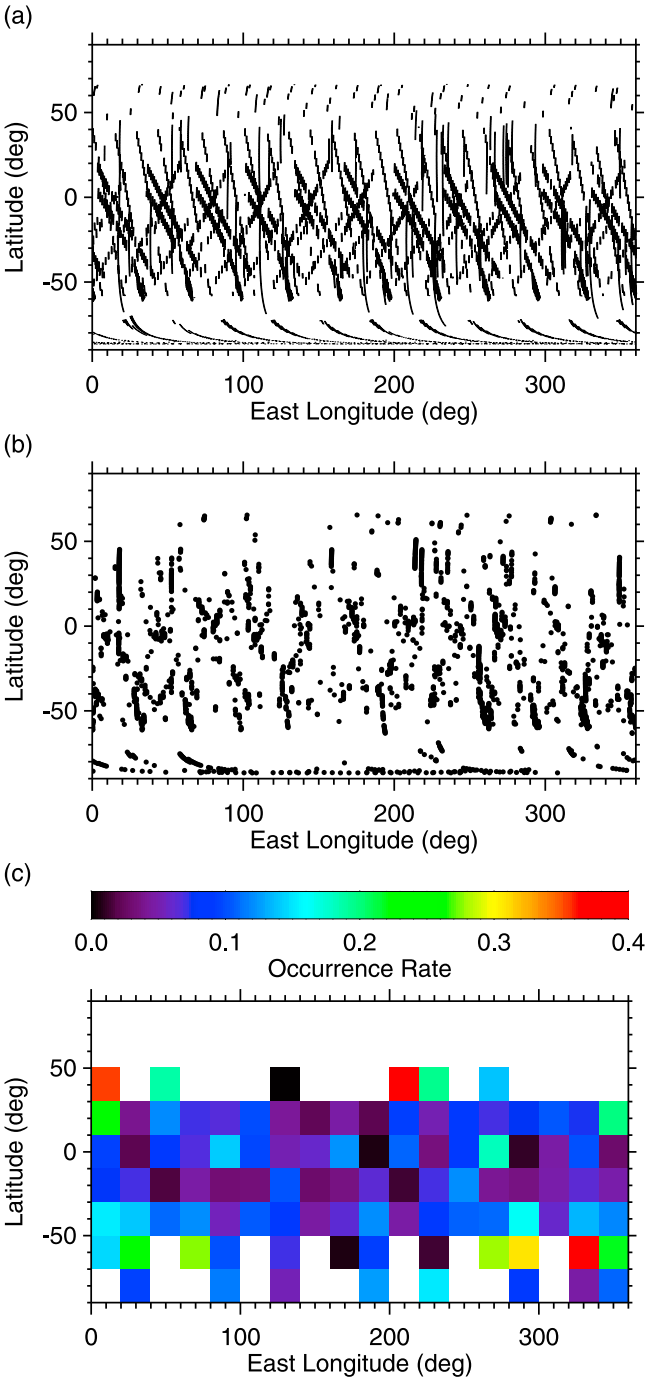


**Figure 2.** (a) Geographic locations sampled by MARSIS at SZA > 107° and at altitude less than 1100 km. (b) Geographic locations where the nightside ionosphere was detected by MARSIS. (c) Occurrence rate map of the nightside ionosphere. Only the bins containing at least 100 measurements are plotted.

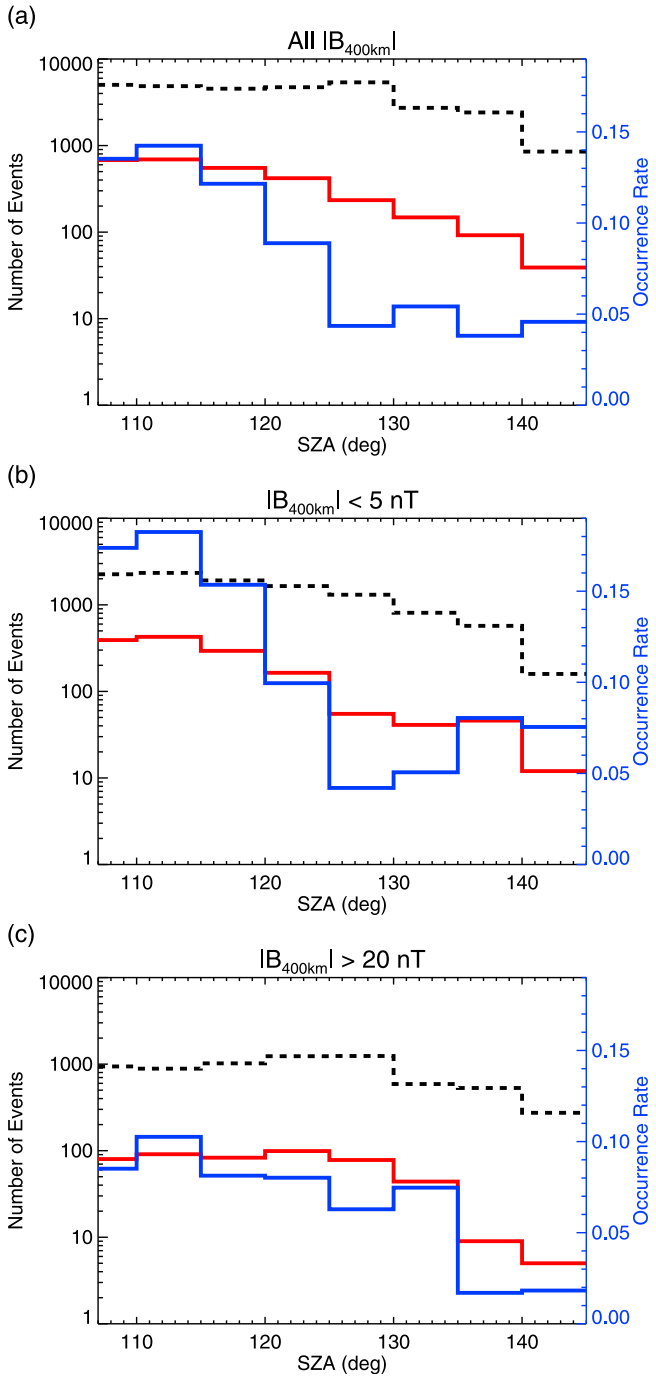


**Figure 3.** (a) Histogram of the occurrence of the nightside ionosphere as a function of SZA. The black dashed histogram represents the total number of observations performed at a given SZA. The red solid histogram shows the number of ionograms containing a signature of the nightside ionosphere. The blue solid histogram traces the occurrence rate of the nightside ionosphere, using the scale on the right. (b) Same as Figure 3a but only for magnitudes of magnetic field lower than 5 nT. (c) Same as Figure 3a but only for magnitudes of magnetic field larger than 20 nT. The magnetic field is computed for the longitude and latitude of Mars Express at 400 km altitude from the model of *Cain et al.* [2003].

than 5 nT), while Figure 3c was obtained for regions with strong crustal magnetic fields (larger than 20 nT). The magnetic field thresholds were chosen as a compromise between a requirement for sufficient number of events in each group of data and for the thresholds to be low/high

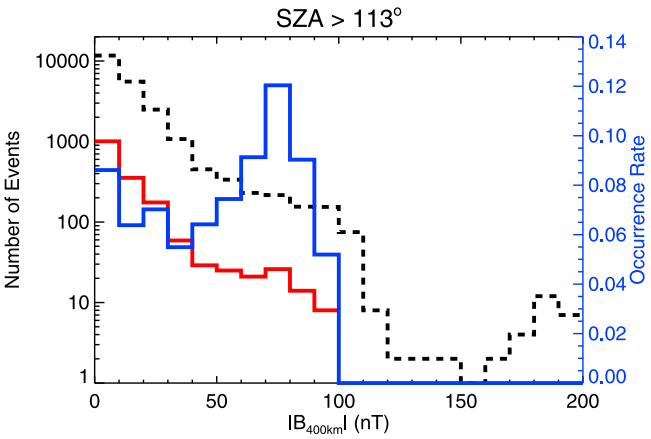


**Figure 4.** Histogram of the occurrence of the nightside ionosphere as a function of the magnetic field magnitude. The meaning of individual histograms is the same as in Figure 3.

enough to clearly separate the data according to the magnetic field magnitude.

[16] In Figure 3a it can be seen that the occurrence rate of the nightside ionosphere is largest for low SZAs and systematically decreases up to SZAs of about 125°. For SZA > 125° it remains nearly constant, at about 5%. Basically, the same dependence is observed in Figure 3b, which was obtained when taking into account only the areas with weak crustal magnetic fields: except that in this case the occurrence rate at low SZAs is larger and the overall dependence is more pronounced. The small increase of the occurrence rate observed at SZA > 135° is possibly just a statistical fluctuation due to the small number of events. The dependence obtained for areas with strong crustal magnetic fields represented in Figure 3c is rather different. One can see that the occurrence rate at low SZAs is significantly lower (about 8%) and does not change much with increasing SZA. There seems to be a sudden decrease of the occurrence rate at SZA > 135°. However, one should remain cautious when interpreting this decrease because the total number of events at such large SZAs is quite low.

[17] Having investigated the dependence on SZA, we shall limit the rest of the study to samples where SZA > 113°. This assures that the ionosphere up to about 300 km altitude is in the shadow of the planet. Furthermore, atmospheric absorption and scattering ensure that the ionosphere is not sunlit up to about 380 km altitude, so that the data analyzed correspond to purely nightside ionosphere with no possible photoionization effects.

[18] A more detailed analysis of the effect of magnetic field magnitude is shown in Figure 4. The meanings of the curves are the same as in Figure 3. There are two noticeable features in the plot. First, the occurrence rate is larger when the magnetic field is less than 10 nT (the first bin of the histogram). This is caused by the large occurrence rate of the nightside ionosphere at low SZAs and is in a good agreement with Figure 3b. Second, the occurrence rate seems to be highest at a magnetic field magnitude of about 75 nT. For larger magnetic field magnitudes the occurrence rate systematically decreases to zero.

[19] Figure 5 illustrates the dependence of the detection and occurrence rates on the inclination of the magnetic field, which is defined as the angle between the local horizontal and the direction of the magnetic field. A value of 0° corresponds to a horizontal magnetic field (i.e., no radial component), while a value of 90° corresponds to a radial magnetic field. Only the measurements performed in areas with reasonably strong magnetic fields (larger than 20 nT) have been taken into account. It can be seen that the occurrence rate of the nightside ionosphere increases as a function of the inclination of the magnetic field, from less than 3% to more than 13%.

[20] In terms of correlation with local time, a dawn-dusk comparison of the occurrence rate of the nightside ionosphere was not possible due to the lack of data in the dawn sector.

### 3.2. Peak Electron Density

[21] As already mentioned in section 2, sounding frequencies larger than the maximum plasma frequency of the ionosphere do not undergo ionospheric reflection. We can convert the maximum reflected plasma frequency for a given ionogram to an ionospheric peak electron density using equation (1). The histogram of peak electron densities obtained from our observations of nightside ionospheric echoes is plotted by the solid curve in Figure 6b. However, since we were able to detect a nightside ionospheric echo in less than 10% of observations, some care is needed to explain why so few nightside ionospheric echoes are observed.

[22] The most probable explanation for the cases in which no ionospheric reflection is detected is that the maximum plasma frequency of the ionosphere is very low and falls below the detection threshold of the MARSIS instrument. The radiated power is very low at low frequencies and decreases as the frequency decreases. This frequency dependence together with the somewhat variable noise level at low frequencies causes the effective low-frequency detection threshold to be rather poorly defined. The best that

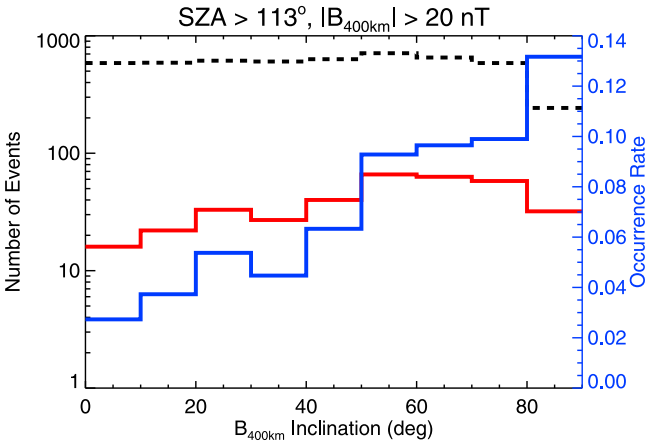


**Figure 5.** Histogram of the occurrence of the nightside ionosphere as a function of the magnetic field inclination. The meaning of individual histograms is the same as in Figure 3.

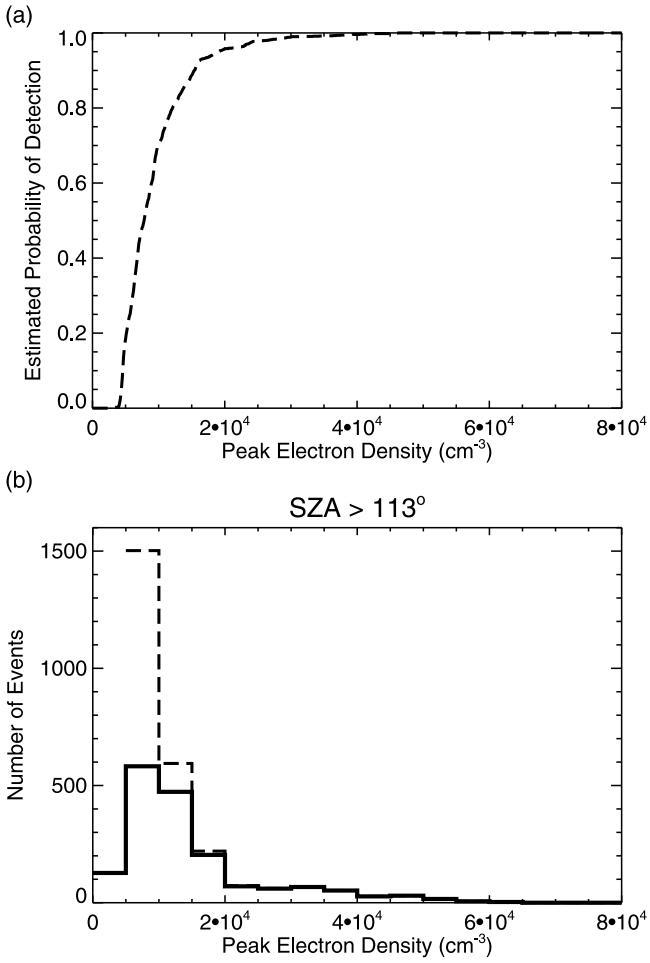


**Figure 6.** (a) Estimated probability of detection of the nightside ionosphere as a function of its peak electron density (see text). (b) Occurrence of the nightside ionosphere as a function of the peak electron density. The solid histogram represents the real number of observed events. The dashed histogram corresponds to the number of events divided by the estimated probability of detection.

we can do is to make a rough estimate of the probability of detection of an existing ionospheric echo as a function of sounding frequency using the actual experimental data. This is possible, because for all of the detected echoes we have recorded not only the maximum but also the minimum frequency of the echo.

[23] For a given frequency we can evaluate the ratio of the number of ionospheric echoes whose minimum frequency is lower than the given frequency to the total number of the analyzed ionospheric echoes. For example, 100% of recorded echoes have a minimum detected frequency lower than that corresponding to $5 \times 10^4$ cm$^{-3}$, 80% have a minimum frequency lower than that corresponding to $1 \times 10^4$ cm$^{-3}$. Assuming the difference between maximum and minimum frequency of an ionospheric echo must be at least 0.11 MHz in order to be observed (which is a rather reasonable value, see Figure 1), we can estimate the probability of detection of an ionospheric echo as a function of peak electron density in the ionosphere. The resulting dependence is shown by the dashed curve in Figure 6a. It can be seen that for peak electron densities above about $1 \times 10^4$ cm$^{-3}$, the probability of detection is 0.75 or greater, but for lower peak electron densities it decreases rapidly. We have used this result to estimate the correct distribution of peak electron densities. The dashed histogram in Figure 6b shows the actual number of detections divided by the probability of detection as described above. The total number of events in the dashed histogram is close to the total number of measurements, indicating that all the events with no identified ionospheric echo can be explained in this simple way. However, it should be noted that about 90% of the events are located in the first bin of the dashed histogram ($n_e < 5000$ cm$^{-3}$). The number of events in this bin reaches far beyond the scale of the histogram. Moreover, the probability of detection of such low densities is so close to zero that it is just a very rough estimate. We have thus decided not to plot the dashed histogram in the lowest bin.

### 3.3. Altitude of the Peak Electron Density

[24] The last piece of information that can be obtained from the nightside ionospheric echoes is the time delay $\Delta t$ between the transmission of a sounding signal and detection of the reflected signal. The first important point is that (unlike the time delay of a typical dayside ionospheric echo [see, e.g., *Gurnett et al.*, 2005]) time delays of nightside ionospheric echoes are usually constant over the frequency range where they are observed. This indicates that the ionospheric reflection takes place always at about the same altitude independent of the sounding frequency, meaning that the nightside ionosphere has a sharp upper edge that is independent of frequency. A histogram of apparent altitudes

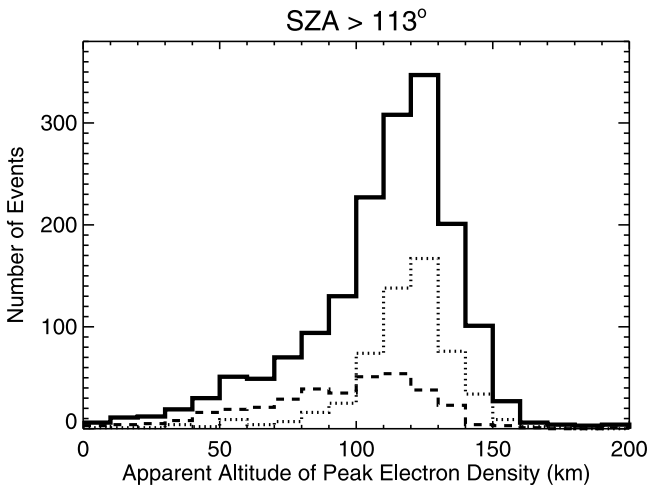


**Figure 7.** Histogram of apparent altitudes of observed peak electron densities. The dotted histogram was obtained when taking into account only the measurements performed at SZA < 125° in areas with weak crustal magnetic fields. The dashed histogram was obtained when taking into account only the measurements performed in areas with strong crustal magnetic fields.

of the peak electron density $z_{peak}$ is shown in Figure 7. Here, $z_{peak}$ is given by

$$z_{peak} = z_{sat} - c\Delta t/2 \quad (2)$$

where $z_{sat}$ is the altitude of the satellite and $c$ is the speed of light in vacuum. The dotted histogram was obtained when taking into account only the measurements performed at SZA < 125° in areas with weak crustal magnetic fields (lower than 5 nT). The dashed histogram was obtained when taking into account only the measurements performed in areas with strong crustal magnetic fields (larger than 20 nT). It can be seen that the interval of apparent altitudes corresponding to the measurements performed in areas with strong crustal magnetic fields is significantly larger (the histogram exhibits a broad peak centered at about 110 km) as compared to the well pronounced maximum at about 125 km obtained for SZA < 125° and weak crustal magnetic fields.

[25] However, a proper determination of the altitude of the peak electron densities is a bit more complicated, because due to the dispersion properties of the plasma medium the sounding signal propagates at a speed lower than the vacuum speed of light. This speed depends on the plasma frequency and varies as a function of altitude. There are well established methods of solving this problem [see, e.g., *Morgan et al.*, 2008, and references therein]. What is important for the present paper is that such an inversion can be carried out. However, a few more assumptions must be made. First, it is necessary to assume that $z$ as a function of $f_p$ is monotonic. Second, an integrable functional form has to be chosen and applied to each interval between sounding points. Following *Morgan et al.* [2008] we assume that $f_p(z)$ is an exponential function of $z$ in each of the intervals. The only exception is the first sounding interval where we assume a constant plasma frequency $f_p = f_p^{local}$. This corresponds to the situation of an abrupt slab-like ionosphere which would explain the nearly horizontal echoes observed. It turns out that the corrected altitudes are only slightly larger than the apparent altitudes, and so are not shown.

## 4. Discussion

[26] We were able to identify ionospheric echoes in about 9% of the verified nightside ionograms. The events for which it was not possible to identify an ionospheric echo may have two possible reasons, both connected and originating from the instrumental limitations of MARSIS. First, electron cyclotron echoes [*Gurnett et al.*, 2005], as well as other types of noise are often detected at lower frequencies, which tends to mask the ionospheric echo. Second, the power of radiated sounding signal significantly decreases at frequencies below about 500 kHz, which makes it impossible to detect echoes if the density is too low. Nightside ionospheres with peak electron densities below about 5000 $cm^{-3}$ are consequently very unlikely to be detected by MARSIS, as shown in Figure 6a. The occurrence rate of the nightside ionosphere resulting from MARSIS measurements can be thus interpreted in terms of "how often the peak density in the ionosphere is large enough to be detected".

[27] The fact that time delays, $\Delta t$, of the observed nightside ionospheric echoes are nearly constant as a function of the sounding frequency strongly suggests that the nightside ionosphere has very "sharp" upper edge: the ionospheric density remains nearly constant down to relatively low altitudes and then increases steeply up to the peak value. Such an ionospheric profile is rather different from typical ionospheric profiles observed on the dayside [*Morgan et al.*, 2008], but is in quite good agreement with electron density profiles observed by *Duru et al.* [2008] at altitudes larger than about 550 km. We believe that this difference can be at least partially explained by a lower temperature (and consequently also lower scale height) in the nightside regions due to the lack of direct solar radiation. However, model ionospheric profiles [*Fillingim et al.*, 2007] suggest that there are probably significant electron densities in the topside of the ionosphere that we miss because of the lower detection limit of the MARSIS instrument. Bottom parts of ionospheric echoes corresponding to larger time delays are usually diffuse, i.e., fuzzy and not very well defined, indicating complicated oblique reflections of the sounding signal. This suggests that the ionosphere is rather structured, possibly with holes similar to those observed at the nightside of Venus [*Gurnett et al.*, 2008].

[28] The dependence of the occurrence rate of the nightside ionosphere on SZA for varying magnetic field magnitude shown in Figure 3 can be interpreted in terms of plasma transport from more ionized near-terminator regions. This would result in the decreasing occurrence rate of the nightside ionosphere as a function of SZA, which is exactly the situation that occurs in areas with weak crustal magnetic fields (Figure 3b). The occurrence rate decreases up to SZA = 125° and remains nearly constant at larger values of SZA, suggesting that at very large SZAs plasma transport is no longer an effective mechanism of ionospheric formation. In areas with strong crustal magnetic fields (Figure 3c) the situation is rather different. There seems to be no clear dependence of the occurrence rate on SZA, indicating that strong crustal magnetic fields are capable of retarding plasma transport from lower SZAs. Depending on the magnetic topology of a given crustal magnetic field anomaly, the field may actually enhance transport locally in some places and prevent it in others, but the overall effect is to retard horizontal transport of the plasma. We do not have any explanation for the apparent change of the occurrence rate of the nightside ionosphere in Figures 3b and 3c. We checked whether the data points in these bins correspond to exceptionally large or low values of magnetic field inclination and found no correlation. Taking into account the rather low number of measurements in these regions and the inherent complexity of the nightside ionosphere, this change might be just a statistical fluctuation.

[29] The histogram of the occurrence rate of the nightside ionosphere as a function of magnetic field magnitude represented in Figure 4 shows that there are no detected nightside ionospheres in areas with very strong crustal magnetic fields (larger than 100 nT). Since plasma transport from the dayside does not seem to play an important role in such areas, the only possible ionization source is probably impact ionization by precipitating electrons [*Fox et al.*, 1993; *Lillis et al.*, 2009]. However, *Brain et al.* [2007] have shown that the flux of 95–148 eV electrons is strongly dependent on the magnetic field topology. In some locations near the strongest crustal magnetic field 100% of

their measurements can be classified as "plasma voids", meaning that there is virtually no electron flux present. This indicates that the field lines in these regions are always closed and seems to be very consistent with our results, explaining the lack of nightside ionospheric echoes in areas with very strong crustal magnetic fields. Although the magnetic field topology may be opened in some areas with the strongest crustal magnetic field, such regions are very small and localized, so we most likely miss them with the relatively small number of total echoes.

[30] Figure 5 demonstrates that in areas with reasonably strong crustal magnetic fields (larger than 20 nT) the orientation of the magnetic field can be used as a proxy for the magnetic field topology, being the crucial parameter controlling the formation of the nightside ionosphere. The occurrence rate in areas with radially oriented magnetic field is more than 4 times larger than in areas with horizontal magnetic field. This is in good agreement with total electron content measurements reported by *Safaeinili et al.* [2007] and can most probably be explained in terms of impact ionization by precipitating electrons affected by crustal magnetic fields. It is suggested that the magnetic field lines in regions of large inclination are open field lines, enabling easy access of incoming suprathermal electrons [*Lillis et al.*, 2004; *Brain et al.*, 2007].

[31] The peak electron density of the ionosphere can in principle be easily determined from the MARSIS instrument using the maximum frequency of the ionospheric echo. However, it is rather tricky to reconstruct a histogram of the peak densities in the nightside ionosphere using these data, because the efficiency of detection of low peak electron densities is very low (see Figure 6). We have tried to compensate for this effect by using the estimated probability of detection of the nightside ionosphere as a function of its peak electron density. We believe that the resulting dashed histogram in Figure 6 expresses the real peak electron densities as well as can be estimated. We would like to mention two main conclusions that can be drawn from this histogram: (1) most of the nightside ionospheres (about 90%) have peak electron density lower than 5000 $cm^{-3}$, which is the approximate lower detection limit of the MARSIS instrument and (2) less than 2% of the events have peak electron densities larger than $1.9 \times 10^4$ $cm^{-3}$, which is the upper limit predicted by *Fox et al.* [1993].

[32] The histogram of apparent altitudes of peak electron densities presented in Figure 7 is strongly affected by two factors, both of which cannot be eliminated and cause the obtained altitudes to be lower than the real ones. First, since there are indications that the nightside ionosphere is finely structured, the observed ionospheric echo is presumably often not a direct vertical echo, but rather an oblique one. Because our calculation of the altitude of peak electron density is based on an assumption of vertical propagation of a sounding signal, such a situation would result in the estimated altitude of peak electron density lower than the real one. Second, there is usually quite a large gap between the local plasma frequency at the spacecraft location and the lowest frequency of the observed ionospheric echo. When calculating the corrected altitude of peak electron density, i.e., when taking into account dispersion properties of the plasma medium, one has to make an assumption about the ionospheric profile corresponding to the plasma frequencies in this interval. Our assumption of a constant plasma frequency between the satellite altitude and the altitude corresponding to the first point with valid ionospheric sounding results again in estimated altitudes of peak electron densities being lower than the real ones. However, since no better estimation of altitudes of peak electron densities is possible, the best we can do is to keep in mind that the computed altitudes should be considered only as lower limits. Taking into account that ionospheric peak altitudes below about 120 km are essentially impossible given what is known about the density profile of the Martian ionosphere, the results depicted in Figure 7 should be used only for rough qualitative estimates.

[33] The contention that apparent altitudes of peak electron densities in areas with strong crustal magnetic field are lower is statistically very significant, both Mann-Whitney U-test and Kolmogorov-Smirnov test [*Sheskin*, 2000] yield significance of nearly 100%. However, taking into account their larger spread, the larger apparent altitudes are probably due to oblique ionospheric echoes occurring more often in these regions rather than due to a real change in peak altitude. This is in an agreement with *Lillis et al.* [2009], who does not expect any variability of peak altitude with magnetic field, and indicates that the nightside ionosphere in areas with strong crustal magnetic fields is more structured, containing localized areas of enhanced electron density.

## 5. Conclusions

[34] Results of a systematic study of observations of the nightside Martian ionosphere obtained from the MARSIS instrument on board the Mars Express spacecraft have been presented. Altogether, 30,523 MARSIS ionograms were analyzed at SZA > 107° and $z_{sat} < 1100$ km. Among these, nightside ionospheric echoes were identified in 2857 cases, corresponding to an occurrence rate of about 9%.

[35] Our results show that at locations with weak crustal magnetic fields the occurrence rate of the nightside ionosphere decreases with increasing SZA up to about 125°, suggesting that plasma transport from the dayside plays a crucial role in the formation of the ionosphere. At locations with strong crustal magnetic fields no such dependence on the SZA is observed, indicating that these magnetic fields are able to retard plasma transport processes. In such areas, the inclination of magnetic field becomes a key parameter: the occurrence rate of the nightside ionosphere is more than 4 times larger at locations where the magnetic field is nearly radial than at the locations where the magnetic field is nearly horizontal. Observed peak electron densities are rather low, less than about $2 \times 10^4$ $cm^{-3}$ in the vast majority of cases. Lower limits to the peak altitudes are mostly in the range 100–150 km.

[36] **Acknowledgment.** The research at the University of Iowa was supported by NASA through contract 1224107 from the Jet Propulsion Laboratory.

## References

Brain, D. A., R. J. Lillis, D. L. Mitchell, J. S. Halekas, and R. P. Lin (2007), Electron pitch angle distributions as indicators of magnetic field topology near Mars, *J. Geophys. Res.*, *112*, A09201, doi:10.1029/2007JA012435.

Cain, J. C., B. B. Ferguson, and D. Mozzoni (2003), An n = 90 internal potential function of the Martian crustal magnetic field, *J. Geophys. Res.*, *108*(E2), 5008, doi:10.1029/2000JE001487.

Chapman, S. (1931), The absorption and dissociative or ionizing effect of monochromatic radiation in an atmosphere on a rotating Earth, Part II. Grazing incidence, *Proc. Phys. Soc.*, *43*, 483–501.

Chicarro, A., P. Martin, and R. Trautner (2004), The Mars Express mission: An overview, in *Mars Express: The Scientific Payload*, edited by A. Wilson and A. Chicarro, *Eur. Space Agency Spec. Publ.*, *ESA-SP 1240*, 3–13.

Duru, F., D. A. Gurnett, D. D. Morgan, R. Modolo, A. F. Nagy, and D. Najib (2008), Electron densities in the upper ionosphere of Mars from the excitation of electron plasma oscillations, *J. Geophys. Res.*, *113*, A07302, doi:10.1029/2008JA013073.

Fillingim, M. O., et al. (2007), Model calculations of electron precipitation induced ionization patches on the nightside of Mars, *Geophys. Res. Lett.*, *34*, L12101, doi:10.1029/2007GL029986.

Fox, J. L., J. F. Brannon, and H. S. Porter (1993), Upper limits to the nightside ionosphere of Mars, *Geophys. Res. Lett.*, *20*(13), 1391–1394.

Gurnett, D. A., et al. (2005), Radar soundings of the ionosphere of Mars, *Science*, *310*, 1929–1933.

Gurnett, D. A., et al. (2008), An overview of radar soundings of the Martian ionosphere from the Mars Express spacecraft, *Adv. Space Res.*, *41*, 1335–1346.

Jordan, R., et al. (2009), The Mars express MARSIS sounder instrument, *Planet. Space Sci.*, *57*, 1975–1986, doi:10.1016/j.pss.2009.09.016.

Lillis, R. J., D. L. Mitchell, R. P. Lin, J. E. P. Connerney, and M. H. Acuña (2004), Mapping crustal magnetic fields at Mars using electron reflectometry, *Geophys. Res. Lett.*, *31*, L15702, doi:10.1029/2004GL020189.

Lillis, R. J., M. O. Fillingim, L. M. Peticolas, D. A. Brain, R. P. Lin, and S. W. Bougher (2009), Nightside ionosphere of Mars: Modeling the effects of crustal magnetic fields and electron pitch angle distributions on electron impact ionization, *J. Geophys. Res.*, *114*, E11009, doi:10.1029/2009JE003379.

Morgan, D. D., D. A. Gurnett, D. L. Kirchner, J. L. Fox, E. Nielsen, and J. J. Plaut (2008), Variation of the Martian ionospheric electron density from Mars Express radar soundings, *J. Geophys. Res.*, *113*, A09303, doi:10.1029/2008JA013313.

Picardi, G., et al. (2004), MARSIS: Mars advanced radar for subsurface and ionosphere sounding, in *Mars Express: The Scientific Payload*, edited by A. Wilson and A. Chicarro, *Eur. Space Agency Spec. Publ.*, *ESA-SP 1240*, 51–69.

Piggott, W. R., and K. Rawer (1972), *U.R.S.I. Handbook of Ionogram Interpretation and Reduction*, Elsevier, New York.

Safaeinili, A., W. Kofman, J. Mouginot, Y. Gim, A. Herique, A. B. Ivanov, J. J. Plaut, and G. Picardi (2007), Estimation of the total electron content of the Martian ionosphere using radar sounder surface echoes, *Geophys. Res. Lett.*, *34*, L23204, doi:10.1029/2007GL032154.

Sheskin, D. J. (2000), *Handbook of Parametric and Nonparametric Statistical Procedures*, 2nd ed., CRC Press, Boca Raton, Fla.

Withers, P. (2009), A review of observed variability in the dayside ionosphere of Mars, *Adv. Space Res.*, *44*, 277–307.

Zhang, M. H. G., J. G. Luhmann, and A. J. Kliore (1990), An observational study of the nightside ionospheres of Mars and Venus with radio occultation methods, *J. Geophys. Res.*, *95*(A10), 17,095–17,102.

F. Duru, D. A. Gurnett, D. D. Morgan, and F. Němec, Department of Physics and Astronomy, University of Iowa, Iowa City, IA 52242, USA. (frantisek.nemec@gmail.com)